Super-resolved live imaging of thick biological samples with 3D Random Illumination Microscopy (3D-RIM)

Thomas Mangeat[1,*], Lorry Mazzella[2], Benoît Rogez[2], Guillaume Giroussens[2], Mathilde Bernard[3], Pablo Vargas[3], Marc Allain[2], Simon Labouesse[1], Jérôme Idier[4], Loïc LeGoff[2,*], Anne Sentenac[2,*]

[1]LITC Core Facility, Centre de Biologie Integrative (CBI), CNRS, Université de Toulouse,UT3, Toulouse, France
[2]Aix Marseille Univ, CNRS, Centrale Marseille, Institut Fresnel UMR7249, Turing Center for Living Systems, Marseille, France
[3]Leukomotion Lab, Paris Cité University, INSERM UMR-S1151, CNRS UMR-S8253, Institut Necker Enfants Malades, F-75015 Paris, France
[4]LS2N, CNRS UMR 6004, F44321 Nantes Cedex 3, France

[*]Authors for correspondence: thomas.mangeat@utoulouse.fr, loic.le-goff@univ-amu.fr, anne.sentenac@fresnel.fr

Abstract

Super-resolved volume imaging of thick, live specimens is greatly hampered by sample induced aberrations and out-of-focus fluorescence. In this work, using a combination of speckled illuminations, three-dimensional photon reassignement and variance processing, we obtained volume images with super-resolution (110 nm transverse, 270 nm axial) on thin samples and maintained a high contrast and high resolution level throughout tens of microns of highly aberrant tissues and up to hundreds of microns in collagen scaffolds.

Super-resolved live imaging of thick biological samples, spanning several tens of micrometers, is becoming increasingly important in cell and developmental biology, but remains a major challenge for one-photon fluorescence .microscopy[1, 2]. All techniques are affected by sample-induced aberrations on the detection side. In addition, methods employing uniform illumination suffer from strong out-of-focus fluorescence background, whereas techniques using patterned illumination (such as confocal-related methods, periodic Structured Illumination Microscopy (SIM), and lattice light-sheet microscopy) are impacted by sample-induced scattering and aberrations in the excitation path, which further degrade their resolution as the imaging depth increases. In this work, we present three-dimensional (3D) random illumination microscopy (3D-RIM) a super-resolved widefield microscopy method adapted to volume imaging that is insensitive to aberrations on the excitation side and efficiently removes the out-of-focus fluorescence.

Following RIM strategy[3, 4, 5, 6], 3D-RIM forms a super-resolved volume image of the sample from the variance of multiple low-resolution images recorded under random speckled illuminations. The key feature of 3D-RIM lays in a global 3D data processing that requires 3D low-resolution images, 3D photon reassignement and 3D variance matching. In brief, we take advantage of the information brought about by the out-of-focus photons and exploit the 3D properties of the point spread function and speckle statistics. As the sample should not be moved with respect to the speckled illumination when recording the 3D low-resolution image, a remote focusing unit was introduced in the microscope's detection arm to perform axial scanning, (see Fig. 1a and supplementary methods for details on the experimental set-up and 3D data processing).

We first demonstrate the performance of 3D-RIM on thin biological samples. We imaged FtsZ:GFP fusions in live Streptococcus pneumonia bacteria. The FtsZ protein plays a crucial role in orchestrating bacterial cell division. It assembles into a ring at the future division site, which shrinks as division proceeds. Figure 1b shows vertical cuts (XZ) of such rings at different stages of cell division. 3D-RIM

could visualize well the central hole of vertical rings with an overall diameter close to 300 nm. Figure 1c shows the chromosomes of fixed human cells labelled for DNA. 3D-RIM reconstructions exhibited a better resolution, notably along the optical axis, better contrast, and less noise than 3D-deconvolved widefield images. The rightmost panel in Fig. 1c displays a maximum intensity projection from 3D-RIM, with color encoding position along the optical axis. A 3D representation of the volume image is provided in the supplementary movie 1. The Fourier Ring Correlation (FRC) analysis [7] estimated the transverse and axial resolution to 110 nm and 270 nm, respectively. Thus, on thin samples, 3D-RIM matched the resolution of 3D-SIM[8, 9].

We next explored the ability of 3D-RIM to image thick biological tissues. We considered *Drosophila* embryos immunostained for lamin to outline the nuclear envelopes. We formed a 3D-RIM volume image of the embryo, ranging from 27 to 52 μm in depth. Figure 2a displays a large-scale XY cut of the 3D image at a depth of 40 μm from the coverslip giving a global view of the embryo circumference. The XZ and XY cuts throughout the volume are shown in the supplementary movies 2 and 3. The inset in Fig. 2a provides a maximum intensity projection with color encoding depth, offering a comprehensive view of the nuclei architecture. The transverse and axial resolutions were estimated by FRC to about 180 nm and 450 nm, respectively. For comparison, we also formed a 3D image by translating the sample through the focal plane and stacking the super-resolved, optically sectioned, two-dimensional (2D) reconstructions of regular RIM [3]. As shown in Fig. 2b, in the zoomed insets and the accompanying line profiles along the optical axis (z), 3D-RIM provided a better image contrast and resolution. In Fig. 2c,d, we imaged the submucosa of the mouse intestine stained with WGA to highlight saccharide structures. High-resolution imaging in this tissue is particularly challenging due to the dense fluorescence labeling and the numerous secretory granules, which create an optically scattering environment. We formed a super-resolved 3D-RIM volume image of the tissue from 27 μm to 42 μm of depth from the coverslip. The maximum intensity projection, color-coded for depths, revealed intricate details of the tissue architecture (Fig. 2c). Fig. 2c,d displays XZ cuts of the 3D image and two intensity profiles along the z-axis comparing 3D-RIM and regular RIM. For this densely labeled sample, regular RIM was hampered by the noisy out-of-focus signal in the raw images. The stack of 2D reconstructions was marred by a strong background, making the individual granules hard to distinguish. In contrast, the absence of background due to efficient noise removal and optical sectioning allowed 3D-RIM to delineate the precise shape of individual granules successfully. The transverse and axial resolutions of 3D-RIM were estimated by FRC to 230 nm and 470 nm, respectively.

The robustness of 3D-RIM to aberrations and its efficient out-of-focus fluorescence removal is further evidenced in supplementary movies 4,5, and 6 which show 3D representations of the tubulin in dendritic cells migrating in a collagen gel scaffold. The three volume images taken at 40 μm, 150 μm and 450 μm from the coverslip are well contrasted and, surprisingly, have similar axial resolutions, from 750 nm to 1 μm and same transverse resolutions, about 330 nm. In contrast, the 3D deconvolved widefield image suffers from a strong out-of-focus background, and from a half as good resolution (see supplementary Fig. 1).

Finally, we illustrate in supplementary figure 2 and movies 7, 8, and 9 the ability of 3D-RIM to provide dynamic volume images of live thick specimen. We imaged fixed and live border cells during their migration in the Drosophila egg chamber. Individual actin fiber bundles were remarkably well resolved in fixed border cells 33 to 46 μm from the coverslip (Fig.S2a-c), and, in live egg chambers, actin dynamic protrusions could be followed during the whole migration process (lasting about 30 min and reaching a depth of 65 μm) without bleaching nor apparent phototoxicity (Fig. S2d and movie 9).

In conclusion, by combining the efficiency of a global 3D data processing with the robustness to aberrations, low phototoxicity and ease of use of RIM[3] on living samples, 3D-RIM provides well-contrasted volume images of thick biological samples at resolutions and depths never documented before. This technique opens up new possibilities for investigating subcellular structures and dynamics in intact tissues like developing embryos or organoids.

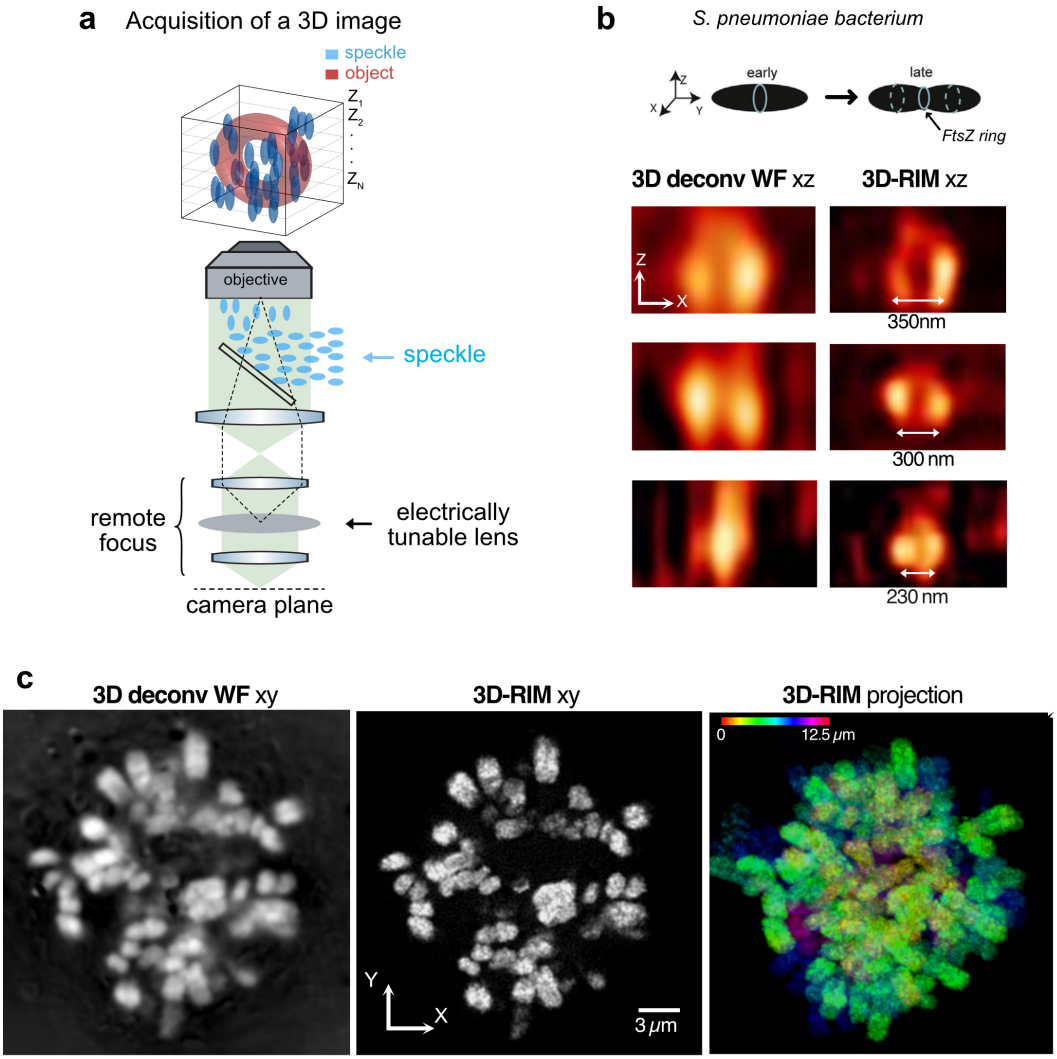

Figure 1: **3D-RIM in single cells.** **a**: Schematic of the 3D-RIM set-up. The sample (here a FtsZ ring) is excited by a speckled illumination. A remote focusing unit, using an electrically tunable lens, permits to record z-stack images while keeping the illumination of the sample unchanged. Multiple (100 to 200) low-resolution 3D speckled images of a sample are recorded under different random speckled illuminations. The super-resolved 3D image is obtained from the variance of the speckled images using a variance matching algorithm (see the methods). **b**: FtsZ:GFP fusion in a live Streptococcus pneumonia bacterium during cell division. Schematic: FtsZ assembles into a ring that gradually shrinks as cytokinesis proceeds. XZ cuts of 3D images of closing rings at three different stages, obtained with 3D-RIM or deconvolved widefield microscopy. In sharp contrast with the deconvolved widefield images, the ring structure is well seen in the 3D-RIM images and the internal hole can even be suspected when the ring structure shrinks to a total diameter of 230 nm. **c**: A fixed human Hep3B cell stained for DNA.The sample is 15 microns thick. From left to right : one XY cut of the deconvolved widefield 3D image, the same cut imaged by 3D-RIM, the maximum intensity projection of the 3D-RIM image with colors encoding Z, see movie 1 for a 3D representation. The 3D-RIM resolution estimated by FRC is 110 nm transversally and 270 nm axially.

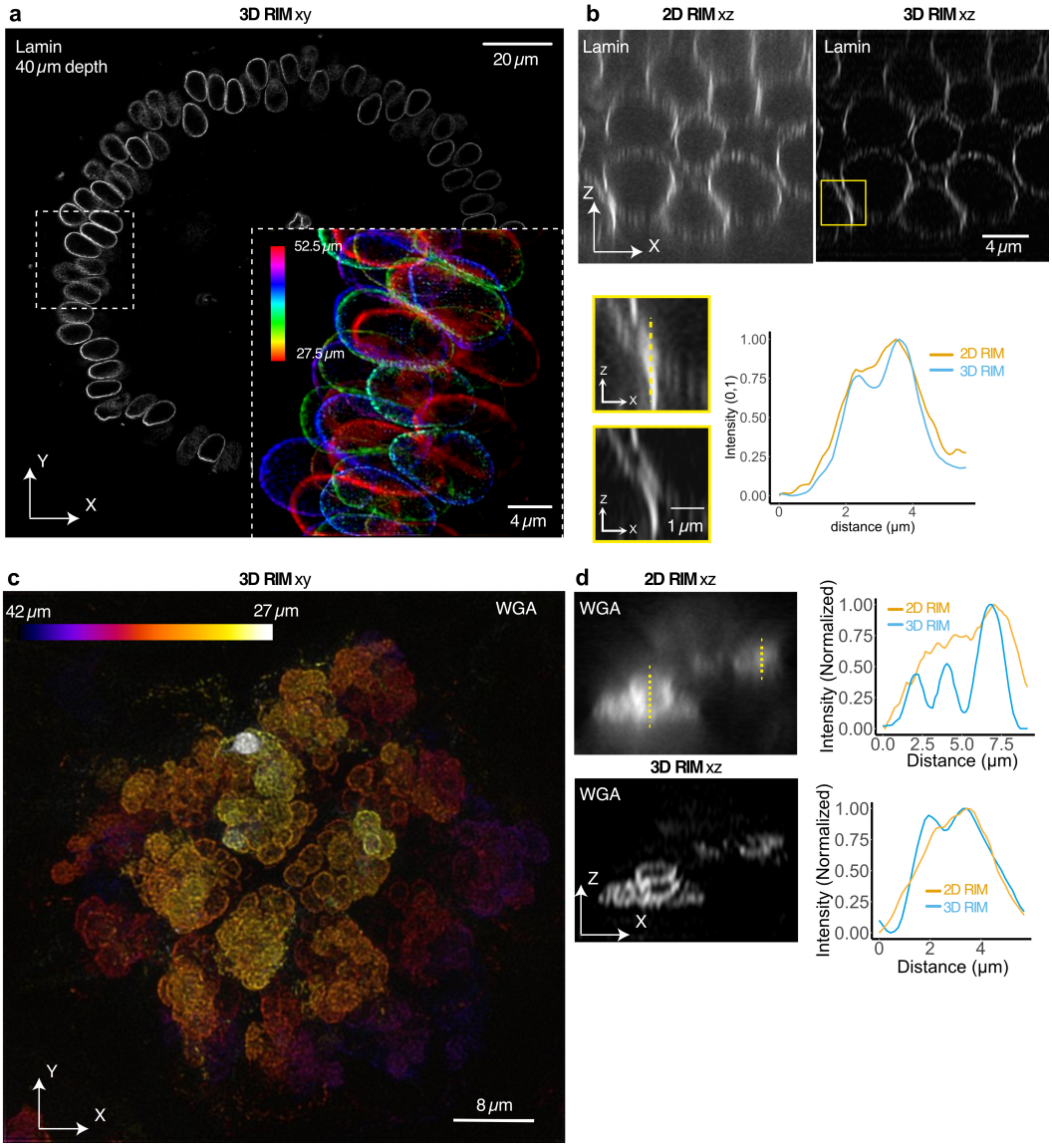

Figure 2: **3D-RIM in thick biological tissues.** **a,b**: *Drosophila* embryo with lamin immunolabeling targeting the nuclear envelopes. **a**: large-scale XY cut of the 3D-RIM image taken 40μm deep from the coverslip. The many nuclei accumulate at the surface of the embryo (see also movies 2,3). The inset shows the maximum intensity projection (colors coding for Z) of a 3D-RIM image spanning from 27 μm to 52 μm from the coverslip. The quality of the reconstruction is maintained throughout the 25 μm of axial scan. The transverse and axial resolutions are estimated by FRC to 180 nm and 450 nm, respectively. **b**: XZ cuts of the 3D images of the same sample obtained with 3D-RIM or regular RIM (2D-RIM). The inset provides zooms on the selected region of interest. The intensity profiles displays the increased resolution of 3D-RIM along the optical axis (Z) (blue line) as compared to regular RIM (orange). **c,d**: Submucosal area of a mouse intestine in which the saccharides are stained with WGA. **c**: Maximum intensity projection of a 3D-RIM image spanning from 27 μm to 42 μm from the coverslip. The transverse and axial resolutions are estimated by FRC to 270 nm and 470 nm, respectively. **d**: Representative XZ cut of the 3D image comparing 3D-RIM with regular RIM (2D RIM). Two intensity profiles along Z are displayed. 3D-RIM clearly outlined the shape of the granules (blue line). Regular RIM was plagued by strong out-of-focus noise (orange line).

Acknowledgments

This work was funded by the following agencies: Agence Nationale de la Recherche (ANR-20-CE45-0024, ANR-22-CE13-0039, ANR-22-CE42-0010, ANR-22-CE42-0026, ANR-24-CE13-2163); Institut Carnot star (3D-RIM).
This project is funded by the « France 2030 » investment plan managed by the French National Research Agency (IDEC, ANR-21-ESRE-0002), and from Excellence Initiative of Aix-Marseille University - A*MIDEX.

References

[1] R. Lin, E. T. Kipreos, J. Zhu, C. H. Khang, and P. Kner, "Subcellular three-dimensional imaging deep through multicellular thick samples by structured illumination microscopy and adaptive optics," *Nature communications*, vol. 12, no. 1, p. 3148, 2021.

[2] Y. Wu, X. Han, Y. Su, M. Glidewell, J. S. Daniels, J. Liu, T. Sengupta, I. Rey-Suarez, R. Fischer, A. Patel, *et al.*, "Multiview confocal super-resolution microscopy," *Nature*, vol. 600, no. 7888, pp. 279–284, 2021.

[3] T. Mangeat, S. Labouesse, M. Allain, A. Negash, E. Martin, A. Guénolé, R. Poincloux, C. Estibal, A. Bouissou, S. Cantaloube, E. Vega, T. Li, C. Rouvière, S. Allart, D. Keller, V. Debarnot, X. B. Wang, G. Michaux, M. Pinot, R. Le Borgne, S. Tournier, M. Suzanne, J. Idier, and A. Sentenac, "Super-resolved live-cell imaging using random illumination microscopy," *Cell Rep. Meth.*, vol. 1, no. 1, p. 100009, 2021.

[4] S. Labouesse, J. Idier, M. Allain, G. Giroussens, T. Mangeat, and A. Sentenac, "Superresolution capacity of variance-based stochastic fluorescence microscopy: From random illumination microscopy to superresolved optical fluctuation imaging," *Physical Review A*, vol. 109, no. 3, p. 033525, 2024.

[5] K. Affannoukoué, S. Labouesse, G. Maire, L. Gallais, J. Savatier, M. Allain, M. Rasedujjaman, L. Legoff, J. Idier, R. Poincloux, *et al.*, "Super-resolved total internal reflection fluorescence microscopy using random illuminations," *Optica*, vol. 10, no. 8, pp. 1009–1017, 2023.

[6] L. Mazzella, T. Mangeat, G. Giroussens, B. Rogez, H. Li, J. Creff, M. Saadaoui, C. Martins, R. Bouzignac, S. Labouesse, *et al.*, "Extended-depth of field random illumination microscopy, edf-rim, provides super-resolved projective imaging," *Light: Science & Applications*, vol. 13, no. 1, p. 285, 2024.

[7] N. Banterle, K. H. Bui, E. A. Lemke, and M. Beck, "Fourier ring correlation as a resolution criterion for super-resolution microscopy," *Journal of structural biology*, vol. 183, no. 3, pp. 363–367, 2013.

[8] M. G. L. Gustafsson, L. Shao, P. M. Carlton, C. J. R. Wang, I. N. Golubovskaya, W. Z. Cande, D. A. Agard, and J. W. Sedat, "Three-dimensional resolution doubling in wide-field fluorescence microscopy by structured illumination," *Biophys. J.*, vol. 94, no. 12, pp. 4957 – 4970, 2008.

[9] L. Shao, P. Kner, E. H. Rego, and M. G. Gustafsson, "Super-resolution 3d microscopy of live whole cells using structured illumination," *Nature methods*, vol. 8, no. 12, pp. 1044–1046, 2011.

[10] G. Giroussens, S. Labouesse, M. Allain, T. Mangeat, L. Mazzella, L. le Goff, A. Sentenac, and J. Idier, "Fast super-resolved reconstructions in fluorescence random illumination microscopy (rim)," *IEEE Transactions on Computational Imaging*, 2024.

[11] H. Kirshner, F. Aguet, D. Sage, and M. Unser, "3-d psf fitting for fluorescence microscopy: implementation and localization application," *Journal of microscopy*, vol. 249, no. 1, pp. 13–25, 2013.

[12] S. Zhou, P. Li, J. Liu, J. Liao, H. Li, L. Chen, Z. Li, Q. Guo, K. Belguise, B. Yi, *et al.*, "Two rac1 pools integrate the direction and coordination of collective cell migration," *Nature communications*, vol. 13, no. 1, p. 6014, 2022.

[13] W. Dai and D. J. Montell, "Live imaging of border cell migration in drosophila," in *Chemotaxis: Methods and Protocols*, pp. 153–168, Springer, 2016.

[14] P. Vargas, P. Maiuri, M. Bretou, P. J. Sáez, P. Pierobon, M. Maurin, M. Chabaud, D. Lankar, D. Obino, E. Terriac, *et al.*, "Innate control of actin nucleation determines two distinct migration behaviours in dendritic cells," *Nature cell biology*, vol. 18, no. 1, pp. 43–53, 2016.

[15] P. J. Sáez, L. Barbier, R. Attia, H.-R. Thiam, M. Piel, and P. Vargas, "Leukocyte migration and deformation in collagen gels and microfabricated constrictions," in *Cell Migration: Methods and Protocols*, pp. 361–373, Springer, 2018.

Methods

3D-RIM data processing

3D-RIM involves the recording of multiple 3D low-resolution images of the sample under different random speckled illuminations. The key requirement of 3D-RIM data processing is that each 3D speckled image I be obtained by keeping the speckled illumination of the sample unchanged so that it can be modeled as the convolution between a 3D point spread function h and the product of the sample 3D fluorescence density ρ and the 3D speckle intensity pattern S,

$$I = h * (\rho \times S). \tag{1}$$

The reconstruction method, 3DalgoRIM, proceeds by first deconvolving the raw images using a 3D Wiener filter, $I' = I * f$ with $\tilde{f}(\boldsymbol{k}) = \tilde{h}^*(\boldsymbol{k})/(|\tilde{h}|^2(\boldsymbol{k}) + \epsilon)$, where $\tilde{a}$ stands for the 3D Fourier transform of a, b^* is the conjugate of b, and ϵ is a Tikhonov parameter that is tuned manually. Then, 3DalgoRIM calculates the empiric variance of the deconvolved speckled images $\widehat{\sigma}^2$. Note that the 3D deconvolution of the raw 3D images is a crucial step. Reassigning the out-of-focus photons to their sources amplifies the peaks of fluorescence intensity stemming from the speckles' hot spots and improves dramatically the signal to noise ratio of the images' variance.
Last, 3DalgoRIM estimates the 3D fluorescence density ρ iteratively so as to minimize the distance between the empirical standard deviation and its theoretical model,

$$L(\rho) = ||\widehat{\sigma}(\boldsymbol{r}) - \sigma(\boldsymbol{r};\rho)||^2 + \mu||\rho||^2 \tag{2}$$

with μ another Tikhonov parameter and $\sigma(\boldsymbol{r};\rho)$ the theoretical standard deviation derived from the asymptotic variance (obtained by assuming an infinite number of speckle realizations),

$$\sigma^2(\boldsymbol{r};\rho) = \int \rho(\boldsymbol{r}')\rho(\boldsymbol{r}'')\Gamma(\boldsymbol{r}'' - \boldsymbol{r}')h'(\boldsymbol{r} - \boldsymbol{r}')h'(\boldsymbol{r} - \boldsymbol{r}'')\mathrm{d}\boldsymbol{r}'\mathrm{d}\boldsymbol{r}'' \tag{3}$$

with $h' = h * f$, Γ the 3D speckle auto-covariance, $\Gamma(\boldsymbol{r}-\boldsymbol{r}') =< (S(\boldsymbol{r}) - < S >)(S(\boldsymbol{r}') - < S >)$ with $<>$ is the averaging over the speckle realizations. Note that the calculation of the 3D theoretical standard deviation is made tractable (and relatively fast) thanks to the orthogonal decomposition of the positive definite operator T defined by $T(u,v) = h(u)h(v)\Gamma(u-v)$ (obtained by Singular Decomposition),

$$T(u,v) = \sum_{n=1}^{N} \eta_n Q_n(u) Q_n(v), \tag{4}$$

where η_n are positive decreasing values. In all the configurations we studied, the first ten terms of the sum were sufficient to get an accurate estimation of σ. The minimization of Eq. (2) is performed with a preconditioned conjugate gradient descent algorithm that is described in detail in [10].

The 2D image reconstructions were also performed by 3DalgoRIM in the same way except that the dimension along the optical axis of h, Γ and ρ was set to one.

In all the reconstructions, the microscope point spread function h and the speckle auto-covariance Γ were estimated using the point spread function generator of Image J (the Gibson-Lanni model)[11] at the illumination or emission wavelengths. The tuning of the Tikhonov parameters ϵ and μ, which depend on the signal to noise ratio of the raw images, is done manually. For all the considered samples, ϵ varied between $5e^{-4}$ and $2e^{-3}$, and μ between $1.6e^{-7}$ and $6e^{-6}$. The iterative process converged in less than 5 iterations.

Experimental set-up

3D-RIM was built using a standard fluorescence microscope (Nikon TiE) in epi configuration. Its key feature lays in the remote focusing unit that permits to produce 3D-stack of images without moving the sample with respect to the illumination. The remote focusing unit consisted of a telecentric 4f relay using two lenses of focal 75mm (AC254-075-A-ML Thorlabs) and 100mm (AC254-100-A-ML Thorlabs) respectively to reimage the intermediate image plane on the camera (Kinetix Scientific Teledyne) and a gravity corrected electrically tunable lens placed in the Fourier plane of the 4f relay (Optotune,

EL-16-40-GTC-VIS-5D-1-C). The optical power of the electrically tunable lens was controlled through an analog signal sent to its controller (Optotune, ICC-1C Controller KIT). Instrument synchronization was controlled with the commercial Inscoper L electronic/software system.

The key feature of the 3D-RIM set-up is the remote focusing unit that permits to record z-stack images while keeping the speckled illumination of the sample unchanged. At this point, it is worth noting that the z-scan is usually performed by translating the sample (or equivalently the objective) through the focal plane. If the illumination is inhomogeneous along the optical axis, as with speckled illumination, translating the sample modifies the way it is illuminated and the image model is not a 3D convolution anymore, which prevents the full application of 3D-RIM data processing. The remote focus unit consisted of a telecentric 4f relay using two lenses of focal 75mm (AC254-075-A-ML Thorlabs) and 100mm (AC254-100-A-ML Thorlabs) to reimage the intermediate image plane on the camera (Kinetix Scientific Teledyne) and a gravity corrected electrically tunable lens placed in the Fourier plane of the 4f relay (Optotune, EL-16-40-GTC-VIS-5D-1-C). The optical power of the electrically tunable lens was controlled through an analog signal sent to its controller (Optotune, ICC-1C Controller KIT).

As changing the z-focus is a limiting factor in the temporal sequence, we recorded P speckled images at a given plane, followed by a z-shift and re-imaging of the same speckle sequence at the new z plane (P=200 on fixed samples and P=100 on live samples). A step of 150 nm was used for the imaging of tissues, Hep3B cells and fixed border cells. A step of 90 nm was used for the FtsZ ring and chromosomes and a step of 250 nm was used for the live imaging of border cells and the imaging of dendritic cells. Typical exposure time for one speckled image section is 10 ms.

Samples preparation

Submucosa of the mouse intestine. Jejunum from one sacrificed mouse was fixed in 4% paraformaldehyde (Electron Microscopy Sciences), washed in PBS, sectioned at $200 - 300\mu m$ thickness, permeabilized with 1% Triton X-100 for 1 h. Saccharides were stained with wheat germ agglutinin (WGA), washed in PBS and mounted in Aqua-Poly-Mount, (PolySciences). Mice were housed and procedures performed in accordance with European and national regulations (Protocol Authorisation APAFIS #38994-2023062718345638). Mice were bred in the CBI Specific and Opportunistic Pathogen Free (SOPF) animal facility. Mice were maintained on a C57Bl/6N genetic background.

***Drosophila* embryo preparation.** We imaged embryos of genotype kuk[EY07696] (Blomington stock #16856), which bear a viable hypomorphic mutation in the gene kugelkern/charleston, responsible for mild nuclear morphology defects. Embryos were collected 2–4 hours after egg laying (AEL), dechorionated in 50% bleach for 2 minutes, fixed in 1 mL of 37% formaldehyde (Sigma-Aldrich, 818708) and 1 mL of heptane for 5 minutes at 4^oC, washed twice in PBS containing 0.3% Triton X-100. Selected embryos were cut in their middle using a microscalpel (Micro Knives–Plastic Handle, 10315-12, F.S.T.), incubated at 4^oC with mouse anti-Lamin antibody (1:10, ADL67.10, DSHB), and 4 hours with goat anti-mouse Alexa Fluor 488 (1:100, Interchim). For imaging, embryo cuts were mounted between two coverslips using a $120\mu m$ deep spacer (Secure-Seal™, Sigma-Aldrich) in Vectashield mounting medium.

Hep3B cell staining. Human hepatocarcinoma cells Hep3B (ATCC HB-8064) were seeded in μ-Dish 35 mm, high Grid-500 (ibidi®, Cat 81166) at 250,000 cells per dish overnight in complete DMEM medium supplemented with 10% of SVF. Cells were fixed with 4% paraformaldehyde in PBS for 10 min at room temperature, extensively washed with PBS before their labeling with DAPI (2 μg/mL) for 10 min in the dark, extensively washed, and imaged.

***Drosophila* border cells migration.** For live imaging, we used the Drosophila stocks slbo::LifeAct–RFP [12] and followed the protocol of Dai and Montell [13]. For fixed imaging conditions, ovaries from Sqh::RLCmyosinII–GFP Drosophila were dissected in Schneider's medium and fixed in 4% paraformaldehyde in phosphate-buffered saline (PBS) for 20 minutes at room temperature. After fixation, the egg chambers were rinsed three times with PBS containing 0.3% Triton X-100 (PBST). The egg chambers were incubated with Alexa-561-conjugated phalloidin (1:100 dilution; Invitrogen, A34055) for 2 hours at room temperature to achieve F-actin staining, followed by three 20-minute washes with PBST.

Dendritic cells in a collagen matrix. Mouse bone marrow-derived dendritic cells (BMDCs) were differentiated and activated with LPS as previously published [14]. Cells were seeded in a collagen gel (2mg/m, type I rat tail collagen, Corning 354249) as described in [15]. The collagen gel was cast in a PDMS-made microfabricated collagen chamber (height=500µm, width=3mm, length=4.5mm). The chemokine CCL19 (80nM, ThermoFischer 250-27B) was added in the cell medium to trigger chemotaxis. After 1 hour of directional migration, cells were fixed with 4%PFA then permeabilized with 0.3%

Triton X-100. Cells were stained for alpha-tubulin (anti-alpha-Tubulin Antibody, Thermofisher, MA1-80017 detected using a AlexaFluor647-coupled anti-rat secondary antibody, Thermofisher, A21472).

Supplementary Figures

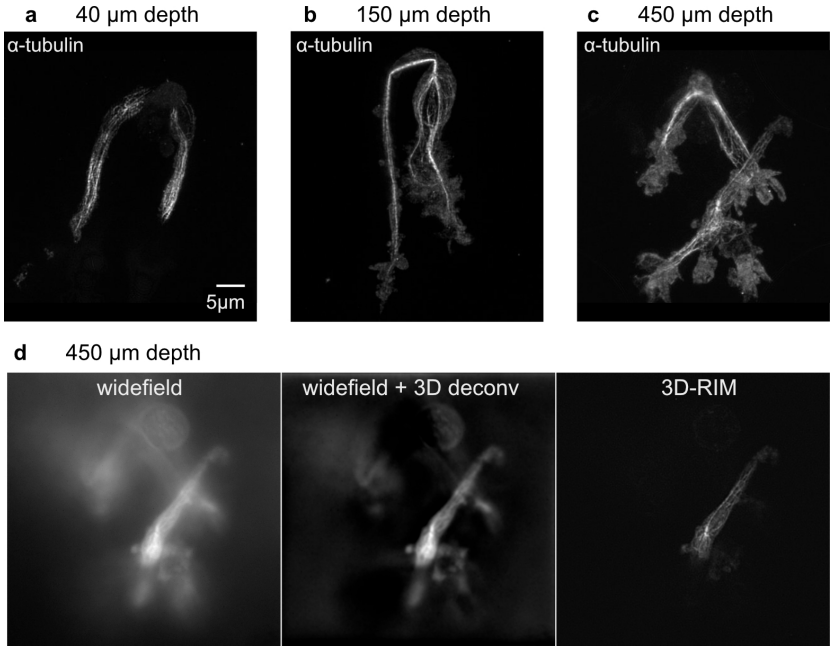

Figure S1: Imaging chemotactic dendritic cells in a collagen scaffold. (a-c)α-tubulin immunofluorescence in mouse bone marrow-derived dendritic cells imaged at different depths (40μm, 150μm and 450μm). Images are maximum intensity projections (see also movies 4,5,6 for a 3D representation). The resolutions of the three volume images, estimated through analysis of the full width at half maximum of the thinnest filaments, is around 330 nm transversally for all depths and ranging from 750 nm at 40 μm to 1000 nm at 150 and 450 μm axially. (d) Comparison of the standard widefield image, 3D-deconvolved widefield image, and 3D-RIM on one section of the cell at 450μm depth. The transverse resolution of the deconvolved widefield image is estimated around 660 nm.

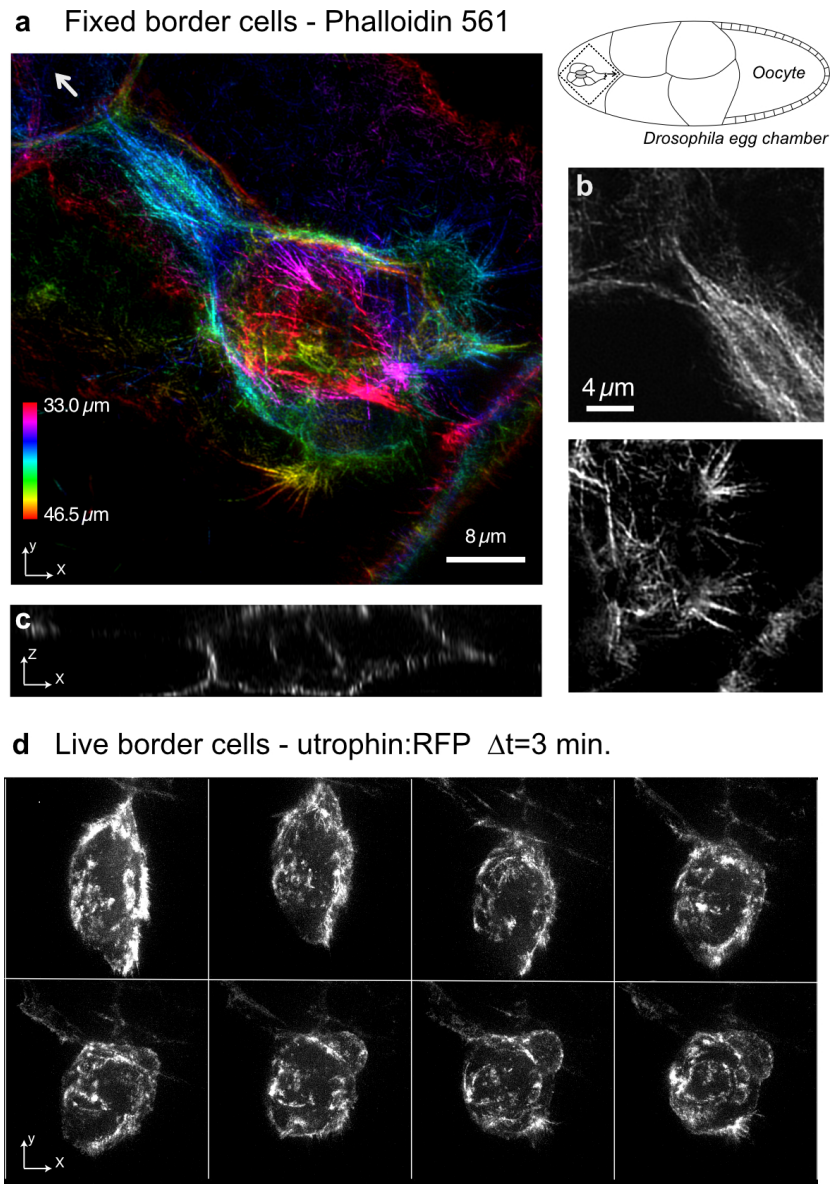

Figure S2: Imaging actin in border cell migration in the *Drosophila* egg chamber. (a-c) Fixed egg chamber with Alexa561 phalloidin staining when the border cells are starting their migration. a: maximum projection with z-encoding colors of the volume image provided in movies 7 and 8. The individual actin bundles are visible throughout the whole border cell cluster, ranging from 33 microns to 46 microns from the coverslip. The schematic on the right shows the structure of the *Drosophila* egg chamber. The dotted square contains the border cells imaged in Fig. S2a. The arrow in the projection and in the schematic shows the direction of migration of border cells, towards the oocyte. b: two XY zooms at different depths and locations. c: one XZ cut of the volume image extracted from movie 7. d: Live 3D imaging of the actin of border cells at the end of their migration when they reach the center of the egg chamber, at a depth of 65 microns from the coverslip (extracted from movie 9). Z-projection of 8 volume images taken three minutes apart.

Supplementary movie captions

Movie 1: 3D representation of DNA in a fixed human cell, associated to Fig. 1c.
Movies 2 and 3 : Full stacks of XY and XZ slices of a volume image of lamin in a fixed *Drosophila* embryo, associated to Fig. 2a.
Movies 4,5,6: 3D representation of the tubulin of fixed dendritic cells, 40 μm, 150 μm and 450 μm deep in a collagen scaffold, respectively. The movies are associated to supplementary Fig. S1
Movies 7 and 8 : Full stacks of XY and XZ slices of the volume image of actin in a fixed *Drosophila* egg chamber, associated to supplementary Fig. S2.
Movie 9: Live volume imaging of actin in a *Drosophila* egg chamber during border cells migration. 3D representation of 8 volume images taken 3 mn apart. The movie is associated to supplementary Fig. S2